

## Spatial variations in the composition of turbidites due to hydrodynamic fractionation

David R. Pyles,<sup>1</sup> Kyle M. Straub,<sup>2</sup> and Jane G. Stammer<sup>1</sup>

Received 17 June 2013; revised 16 July 2013; accepted 18 July 2013.

[1] This study uses measurements from physical experiments to document turbidity currents, which are density currents composed of suspended sediment and water, to be effective at hydrodynamically fractionating minerals on the basis of grain density and grain shape alone, resulting in large-scale spatial variations in the composition of their deposits. While grain composition varies spatially, the population sampled at any one location is hydrodynamically equivalent. Spatial variations in composition of the deposits are modeled using exponential decay functions, which are based on initial concentration of grain types and their respective differences in settling velocity. We further discuss implications of this process for addressing practical geophysical problems, in which mineralogical distributions are important, such as provenance and geochronology studies, subsurface imaging, and predicting bulk properties of subsurface reservoirs. **Citation:** Pyles, D. R., K. M. Straub, and J. G. Stammer (2013), Spatial variations in the composition of turbidites due to hydrodynamic fractionation, *Geophys. Res. Lett.*, 40, doi:10.1002/grl.50767.

### 1. Introduction

[2] Turbidity currents are density currents composed of suspended sediment and water and are the primary mechanism for transporting sediment to submarine fans, which contain channel-lobe elements that form a radially dispersive map pattern [Normark *et al.*, 1979] (Figure 1a). The grain size of turbidite lobes generally decreases toward their lateral and distal margins [Bouma, 1962; Luthi, 1981] (Figure 1b). This pattern results from lateral expansion of the current after it exits the channel and enters the lobe, a region lacking lateral confinement, leading to a spatial decrease in flow velocity and therefore decrease in shear stress and sediment transport capacity [Rouse, 1950]. As settling velocity ( $w_s$ ) is controlled by grain diameter [Stokes, 1851], grains are commonly deposited in the order of decreasing size down current. However, grain density and shape also dictate  $w_s$  [Stokes, 1851; Dietrich, 1982; Ferguson and Church, 2004]. Angular grains have higher drag force ( $F_g$ ), and

therefore lower  $w_s$ , than spheres of equivalent volume, just as spherical, relatively high-density grains have a higher  $w_s$  than spherical lower-density grains of equivalent volume. Critically, each of the common turbidite sandstone-forming minerals such as quartz, feldspar, and mica has a distinctive density due to chemical composition and a distinctive shape partly due to mineral cleavage.

[3] Hydrodynamic fractionation of mineral grains has been a topic of research, particularly for understanding the distribution of placers in rivers [e.g., Rubey, 1933; Slingerland, 1984]; however, no earlier studies document this process in turbidites, although spatial variations in turbidite mineralogy are evident. For example, in 2-D physical experiments, spatial changes in composition are documented [Choux and Druitt, 2002; Choux *et al.*, 2004], although the input grain size distributions for the different particle types were different. In outcrop studies, spatial changes in composition are documented primarily for heavy minerals such as magnetite [e.g., Shideler *et al.*, 1975] over large-scale stratigraphic units such as formations [Lovell, 1969; Shideler *et al.*, 1975], or these studies were only focused on a small part of an individual bed [Norman, 1969] and did not document grain size and shape distributions for each mineral species. In seafloor studies, spatial changes in composition are documented for individual turbidite beds [Sarnthein and Bartolini, 1973; Jones *et al.*, 1992], but input grain size distributions of each grain type were different.

[4] Several commonly addressed geophysical problems are strongly based on mineralogical composition (e.g., provenance, geochronology, subsurface imaging, porosity and permeability, and geomechanical studies). As such, spatial variations in turbidite composition have implications for how these studies are conducted and how the data are interpreted.

[5] Turbidite lobes are optimal for testing how turbidity currents spatially fractionate grains on the basis of grain density and shape as they are net-depositional units and sediment is primarily deposited from suspension [Middleton, 1993]. Due to infrequent occurrence, great water depths, and high velocities, few studies document naturally occurring turbidity currents and their deposits in modern submarine fans [e.g., Hay, 1987]. Outcrop examples of turbidites generally do not have the lateral and longitudinal continuity of bedding sufficient to document composition over the entirety of the deposit, and flow processes are difficult to deduce. However, 3-D flow dynamics, sediment transport, and characteristics of turbidites have successfully been examined at reduced scale for at least three decades [e.g., Luthi, 1981].

[6] Here we use measurements from 3-D physical experiments to test how turbidity currents spatially fractionate sediment on the basis of grain density and shape alone, propose a semiempirical model that can be applied to natural systems, and discuss implications of this process for

Additional supporting information may be found in the online version of this article.

<sup>1</sup>Chevron Center of Research Excellence, Department of Geology and Geological Engineering, Colorado School of Mines, Golden, Colorado, USA.

<sup>2</sup>Department of Earth and Environmental Sciences, Tulane University, New Orleans, Louisiana, USA.

Corresponding author: D. R. Pyles, Chevron Center of Research Excellence, Department of Geology and Geological Engineering, Colorado School of Mines, 1516 Illinois St., Golden, CO 80401, USA. (dpyles@mines.edu)

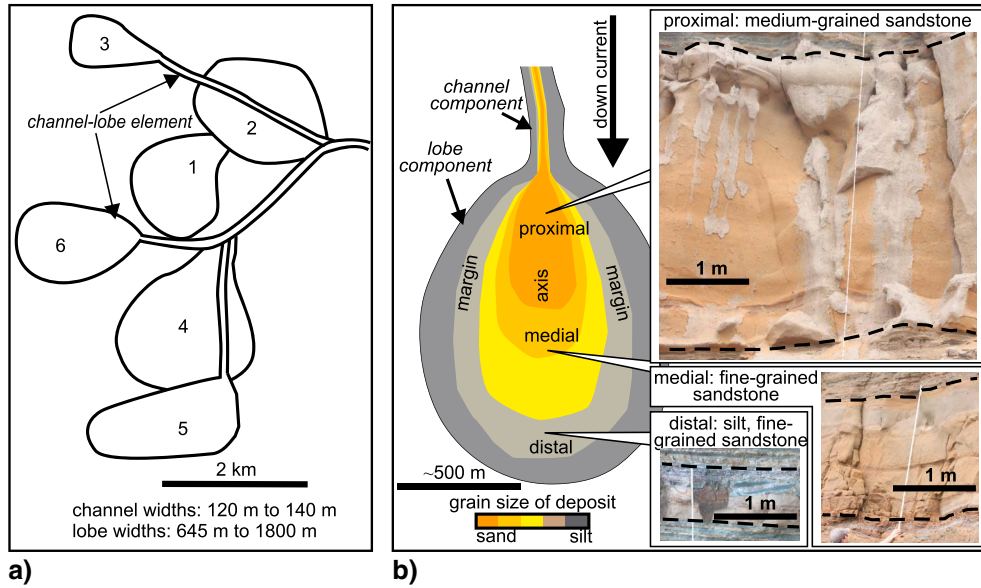


**Figure 1.** (a) Map of the Navy submarine fan, California (from *Normark et al. [1979]*; image reproduced with permission from *Sedimentology*). (b) Diagram and photos of a channel-lobe element from the Point Loma Formation illustrating a longitudinal decrease in the grain size.

addressing some practical geophysical problems where mineralogical composition is important.

**2. Methodology**

[7] Two experiments were conducted in a 6 m long, 4 m wide, and 2.2 m deep basin equipped with an acoustic Doppler profiler (ADP) and a 35 MHz ultrasonic topography scanner (Figure 2). The turbidity currents were composed of a mixture of clear water, dissolved salt ( $\text{CaCl}_2$ ), and suspended sediment and had an excess density of 4% relative to the ambient water in the basin. Of this excess density, 50% was from suspended sediment and 50% was from dissolved salt. The sediment-saltwater mixture was introduced to the basin through a constant head tank, which maintained steady discharge to the basin. Thickness and discharge of all currents at the basin entrance were approximately constant with values of 0.11 m and  $3.0 \times 10^{-3} \text{ m}^3/\text{s}$ , respectively.

The duration of each current was  $255 \pm 47 \text{ s}$ . Once the currents entered the basin, they laterally expanded and flowed down the basin floor which had a 10% slope in the primary flow direction. ADP measurements of flow velocity and thickness just downslope of the entrance box were used to calculate Reynolds ( $Re$ ) and densimetric Froude numbers ( $Fr_D$ ) as 8000 (turbulent) and 0.5 (subcritical), respectively (Table 1). After traversing the  $14.7 \text{ m}^2$  study area, the currents plunged into a moat where perimeter drains removed the currents, preventing reflections. The experimental currents were highly depositional with little-to-no sediment entrainment from the bed. The experiments were conducted at reduced scale relative to submarine transport systems. A comparison of how our model compares to natural settings is listed in Table 1.

[8] Two experiments were performed; each consisted of five turbidity currents that produced stacked successions of lobate turbidites. In the first experiment, the density

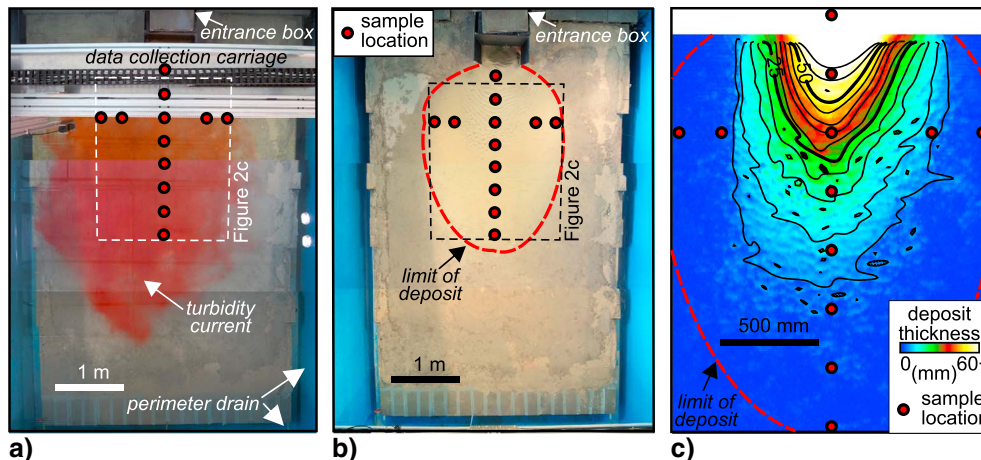


**Figure 2.** Plan view photographs of (a) a turbidity current, (b) resulting deposit, and (c) thickness map from the shape experiment.

**Table 1.** Comparison Between the Experimental Currents and Those in Natural Settings<sup>a</sup>

	Experimental Currents	Scaled to Natural System <sup>b</sup>
$Fr_D$	0.51	0.51
$u$ (m/s)	0.061	0.61
$H$ (m)	0.1	10
$L$ (m)	1.6	4,000
$T$ (min)	5.5	55
$Re$	8,000	6,100,000
D50 ( $\mu\text{m}$ )	112	182

<sup>a</sup> $Fr_D$ =densimetric Froude number,  $u$ =velocity,  $H$ =flow height,  $L$ =flow length,  $T$ =duration of flow,  $Re$ =Reynolds number, D50=median grain diameter.

<sup>b</sup>Scaling calculations included in supporting information.

experiment, 50% of the sediment volume was spherical soda-lime glass ( $r_s=2.5 \text{ g/cm}^3$ ), the control, and 50% was spherical zirconia-silicate glass ( $r_s=3.85 \text{ g/cm}^3$ ) with short-to-long axis ratios of  $0.95 \pm 0.01$  and  $0.93 \pm 0.03$ , respectively (Figure 3a). In the second experiment, the shape experiment, 50% of the sediment volume was spherical soda-lime glass ( $r_s=2.5 \text{ g/cm}^3$ ), the control, and 50% was angular soda-lime glass ( $r_s=2.5 \text{ g/cm}^3$ ), with short-to-long axis ratios of  $0.95 \pm 0.01$  and  $0.44 \pm 0.01$ , respectively (Figure 3a). The nominal grain-size distributions of the three sediment types were similar, ranging from 101 to 141  $\mu\text{m}$  for the D50, and 27 to 62  $\mu\text{m}$  for the standard deviation.

[9] Thickness maps (Figure 2) were produced using a topography scanner, which scanned the basin bathymetry before and after each experiment using a common 5 mm (latitude) by 10 mm (longitude) grid.

[10] Samples from the deposits of the experiments were manually collected along a cross-shaped grid (Figure 2). Samples were split into 1 g aliquots and graphite particles were added to each sample at a 2:1 ratio, to spatially separate the sampled grains. The sediment-graphite mixture was mounted into 30 mm diameter cups and mixed with epoxy resin. Finally, the samples were polished to a 1  $\mu\text{m}$  finish.

[11] Samples were analyzed with a quantitative and automated scanning electron microscope. Backscatter electron images were acquired over an area of 4  $\text{cm}^2$  with 2  $\mu\text{m}$  resolution for each sample. The three grain types were quantitatively differentiated using imaged-based software. In the density experiment, zirconia-silicate glass grains are denser and create a brighter backscatter image than soda-lime

glass grains, whereas in the shape experiment, the two grain types have distinctive shapes (Figure 3a).

[12] A more detailed description of the experimental design, calculations of scale, and description and operating conditions for measuring composition are included in the supporting information.

### 3. Results

[13] The deposits of both experiments were lobate and unchannelized in plan view, had a thick axis, and strata thinned radially away from the sediment source (Figure 2). More than 99% of input sediment was deposited on the basin floor. The shapes of the experimental deposits were similar to lobes deposited in distributive submarine fan settings (Figure 1).

[14] Large-scale variations in the composition of the experimental deposits are documented (Figure 3b). In the density experiment, the concentration by volume of high-density grains decreased by more than  $\sim 50\%$  along the longitudinal transect and similarly from the axis of the deposit to its lateral margins. In the shape experiment, the concentration of angular grains increased by  $\sim 60\%$  along the longitudinal profile and similarly from the axis of the deposit to its lateral margins.

[15] Figure 4 documents grain-size distributions for a representative sample in the density experiment. In this sample, low-density grains are coarser than high-density grains, although when the populations are normalized by calculated  $w_s$  [Ferguson and Church, 2004, equation 4], the plots approximately align, meaning the  $w_s$  of each population are approximately the same or hydraulically equivalent (in the sense of Rubey [1933]).

[16] These results indicate that  $w_s$  is a primary control on the spatial distributions in concentration ( $C$ ), which are semiempirically modeled as

$$C(x_{\text{norm}}) = C_0 e^{-\Delta w_s x_{\text{norm}}}, \text{ for } \Delta w_s \geq 0 \quad (1)$$

$$C(x_{\text{norm}}) = (1 - C_0) - e^{\Delta w_s x_{\text{norm}}}, \text{ for } \Delta w_s \leq 0, \quad (2)$$

where  $C_0$  is the initial concentration by volume of the tested grains relative to tested and control grains ( $(V_i / (V_i + V_c))$ ; 0.5 for these experiments),  $\Delta w_s$  is the difference between the settling velocities of the tested and control grains ( $(w_s - w_{sc}) / w_{sc}$ ; 0.95 for the density experiment and  $-0.25$  for the shape experiment), and  $x_{\text{norm}}$  is the normalized distance  $(x/x_{\text{tot}}) - x_{\text{tot}}$  is where  $>99\%$  of the sediment

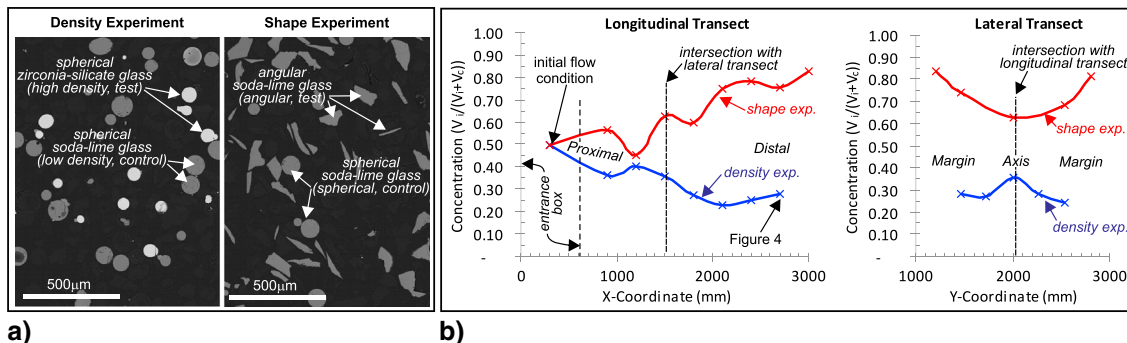


**Figure 3.** (a) Scanning electron microscopy images of samples from each experiment. (b) Graphs documenting (left) longitudinal and (right) lateral changes in the concentration by volume of the experimental deposits. The locations of samples from the shape experiment are shown in Figure 2.

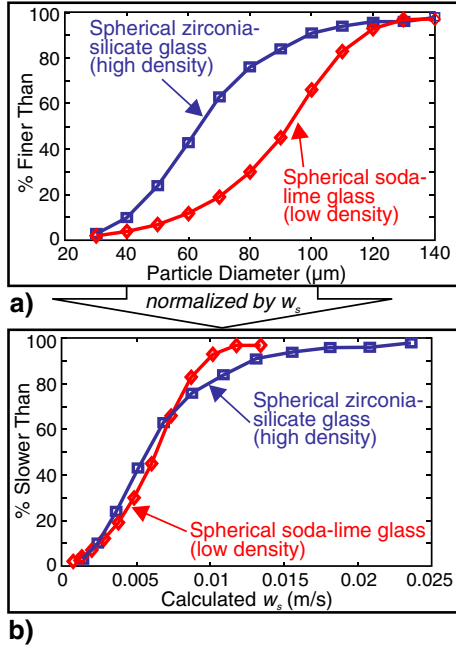


**Figure 4.** (a) Grain size distributions of high- and low-density grains for one sample from the density experiment (sample  $x = 2700$ ,  $y = 2000$ ; location of the sample shown in Figure 3). (b) Calculated  $w_s$  distributions for the same sample.

volume is surpassed (99.4% for the density experiment and 99.7% for the shape experiment). Exponential decay functions were chosen because they are dependent on initial conditions ( $C_0$ ), conserve mass, and assume no bed entrainment. The predicted values are approximately aligned with measured values ( $0.89 \leq r \leq 0.92$ ), indicating that the equations work reasonably well within  $\Delta w_s$  values of the experiments ( $-0.28 \leq \Delta w_s \leq 0.80$ ; Figure 5a). Figure 5b shows predicted concentration trends and both halving and doubling length scales for a range of  $\Delta w_s$  values.

#### 4. Discussion and Conclusions

[17] Results from this study might underrepresent the amount of fractionation that occurs in nature. In a sensitivity analysis of  $w_s$ , using *Ferguson and Church* [2004, equation 4], we document that shape has the greatest influence on  $w_s$  for grains larger than  $\sim 100 \mu\text{m}$ , whereas density has the

greatest influence on  $w_s$  for grains smaller than  $\sim 100 \mu\text{m}$  in diameter. This transition occurs where particle Reynolds numbers become turbulent ( $Re_p \approx 1$ ). Our experiments used grain sizes that straddled these changes. Grain sizes in natural turbidites range from clay ( $\sim 0.04 \mu\text{m}$ ) to pebbles ( $> 4000 \mu\text{m}$ ). As such, fractionation due to grain shape and density could be enhanced for relatively coarse-grained and fine-grained turbidites, respectively. Furthermore, the experimental turbidity currents did not entrain sediment from the bed, as they do in natural settings. If entrainment favored angular and low-density grains, this process could enhance fractionation.

[18] Suspended silt and clay grains enhance the effective density of turbidity currents, serving to increase their mobility and the depositional area of their deposits [*Gladstone et al.*, 1998; *Salaheldin et al.*, 2000]. Sand-sized grains of relatively low density have the same affect [*Hodson and Alexander*, 2010]. The area of the turbidite lobe in the shape experiment is  $\sim 50\%$  larger than that of the density experiment, although both contain similar amounts of sediment. We therefore propose that angular, sand-sized grains suspended in turbidity currents can offer similar hydrodynamic benefits as silt, clay, and low-density particles.

[19] Spatial changes in the composition of turbidite lobes due to hydrodynamic fractionation have implications for addressing many practical geophysical problems. First, turbidites are commonly used in provenance and geochronology studies, and samples from different parts of a turbidite could plot in different domains of a quartz-feldspar-lithic ternary diagram, which is one method for interpreting source terrain [*Dickinson et al.*, 1983]. Also, different zircon and apatite grain sizes can be derived from different aged source areas [e.g., *Lawrence et al.*, 2011]. Second, spatial changes in composition have implications for interpreting subsurface images as changes in density due to composition can affect resistivity, neutron density, and gamma ray logs [*Asquith and Gibson*, 1982] and seismic reflection amplitude of the deposit [*Bachrach and Mukerji*, 2004]. Third, spatial changes in composition can affect bulk properties that influence the storage capacity and recoverability of fluids in subsurface reservoirs. For example, enhanced concentrations of angular particles such as volcanic glass and biotite in distal, although sand-rich, parts of turbidites affect secondary porosity and permeability as these grains characteristically alter to zeolite cements and clay during diagenesis, causing a reduction in porosity and permeability [*Beard and Weyl*,

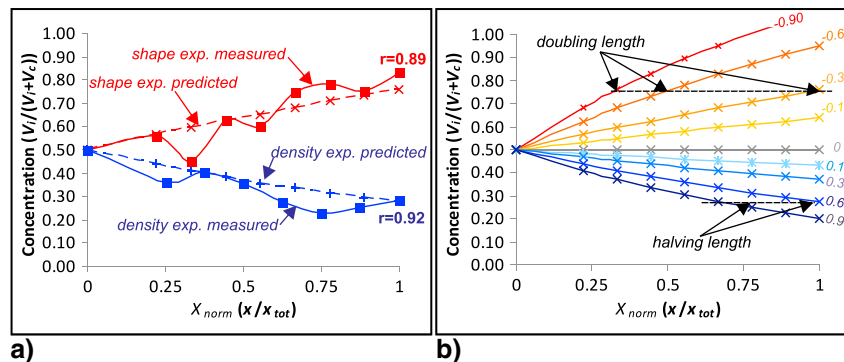


**Figure 5.** (a) Graph comparing measured and predicted (using equations (1) and (2)) spatial changes in composition. (b) Predicted spatial changes in composition using a range of  $\Delta w_s$  values; halving and doubling lengths are labeled.

1973]. Also, spatial changes in mineralogy can result in differential compaction as rigid grains such as quartz compact differently than angular, labile grains such as mica, resulting in spatial changes in porosity [Krumbein and Monk, 1942]. Additionally, geomechanical properties such as Young's modulus and Poisson's ratio are related to mineralogical composition and determine the fracturability of sedimentary deposits [Harris et al., 2011].

[20] In conclusion, this study documents turbidity currents to be effective at hydrodynamically fractionating grains on the basis of grain density and shape, resulting in large-scale spatial variations in the composition of their deposits. This process has implications for addressing practical geophysical problems.

[21] **Acknowledgments.** Funding for this study was provided by Chevron. Mineralogical analyses were conducted at Whiting Petroleum. The manuscript benefited from constructive reviews by B. Cardenas, M. Lamb, and P. Myrow. We thank J. Kuykendall, who was instrumental in preparing the experimental facility for this study, and C. Esposito who assisted in running the experiments.

[22] The Editor thanks an anonymous reviewer and Paul Myrow for their assistance evaluating this paper.

## References

- Asquith, G., and C. Gibson (1982), *Basic Well Log Analysis for Geologists*, American Association of Petroleum Geologists, Tulsa, Oklahoma, 216 pp.
- Bachrach, R., and T. Mukerji (2004), The effect of texture and porosity on seismic reflection amplitude in granular sediments: Theory and examples from a high-resolution shallow seismic experiment, *Geophysics*, *69*, 1513–152.
- Beard, D. C., and P. K. Weyl (1973), Influence of texture on porosity and permeability of unconsolidated sand, *Am. Assoc. Pet. Geol. Bull.*, *57*, 349–369.
- Bouma, A. H. (1962), *Sedimentology of Some Flysch Deposits: A Graphic Approach to Facies Interpretations*, Elsevier, Amsterdam, 168 p.
- Choux, C., and T. Druitt (2002), Analogue study of particle segregation in pyroclastic density currents, with implications for the emplacement mechanisms of large ignimbrites, *Sedimentology*, *49*, 907–928.
- Choux, C., T. Druitt, and N. Thomas (2004), Stratification and particle segregation in flowing polydisperse suspensions, with applications to the transport and sedimentation of pyroclastic density currents, *Journal of Volcanology and Geothermal Research*, *138*, 223–241.
- Dickinson, W. R., L. S. Beard, G. R. Brakenridge, J. L. Erjavec, R. C. Ferguson, K. F. Inman, R. A. Knepp, F. A. Lindberg, and P. T. Ryberg (1983), Provenance of North American Phanerozoic sandstone in relation to tectonic setting, *Geol. Soc. Am. Bull.*, *94*, 222–235.
- Dietrich, W. E. (1982), Settling velocity of natural particles, *Water Resour. Res.*, *18*, 1615–1626.
- Ferguson, R. I., and M. A. Church (2004), Simple universal equation for grain settling velocity, *J. Sediment. Petrol.*, *74*, 933–937.
- Gladstone, C., J. C. Phillips, and R. S. J. Sparks (1998), Experiments on bidisperse, constant-volume gravity currents: Propagation and sediment deposition, *Sedimentology*, *45*, 833–843.
- Harris, N. B., J. L. Miskimins, and C. A. Mnich (2011), Mechanical anisotropy in the Woodford Shale, Permian Basin: Origin, magnitude, and scale, *The Leading Edge*, *30*, 284–291.
- Hay, A. E. (1987), Turbidity currents and submarine channel formation in Rupert Inlet, British Columbia. 2. The role of continuous and surge-type flow, *J. Geophys. Res.*, *92*, 2883–2900.
- Hodson, J. M., and J. Alexander (2010), The effect of grain-density variation on turbidity currents and some implications for the deposition of carbonate turbidites, *J. Sediment. Petrol.*, *80*, 515–528.
- Jones, K. P. N., I. N. McCave, and P. P. E. Weaver (1992), Textural and dispersal patterns of thick mud turbidites from Madeira Abyssal Plain, *Mar. Geol.*, *107*, 149–173.
- Krumbein, W. C., and G. D. Monk (1942), Permeability as a function of the size parameters of unconsolidated sand, *Petroleum Technology*, AIME Technical Publication 1492, v. 5, 1–11.
- Lawrence, R. L., R. Cox, R. W. Mapes, and D. S. Coleman (2011), Hydrodynamic fractionation of zircon age populations, *Geol. Soc. Am. Bull.*, *123*, 295–305.
- Lovell, J. P. B. (1969), Tyee Formation: A study of proximity in turbidites, *J. Sediment. Petrol.*, *39*, 935–953.
- Luthi, S. (1981), Experiments on non-channelized turbidity currents, *Mar. Geol.*, *40*, 59–68.
- Middleton, G. V. (1993), Sediment deposition from turbidity currents, *Annu. Rev. Earth Planet. Sci.*, *21*, 89–114.
- Norman, T. N. (1969), A method to study the distribution of heavy-mineral grain abundance in a turbidite, *Sedimentology*, *13*, 236–280.
- Normark, W. R., D. J. Piper, and G. R. Hess (1979), Distributary channels, sand lobes, and mesotopography of Navy Submarine Fan, California Borderland, with applications to ancient fan sediments, *Sedimentology*, *26*, 749–774.
- Rouse, H. (Ed) (1950), *Engineering Hydraulics*, John Wiley and Sons, New York, 1039.
- Rubey, W. W. (1933), The size-distribution of heavy minerals within a water-laid sandstone, *J. Sediment. Petrol.*, *3*, 3–29.
- Salaheldin, T. M., J. Imran, M. H. Chaudhry, and C. Reed (2000), Role of fine-grained sediment in turbidity current flow dynamics and resulting deposits, *Mar. Geol.*, *171*, 21–38.
- Samthein, M., and C. Bartolini (1973), Grain size studies on turbidite components from Tyrrhenian deep sea cores, *Sedimentology*, *20*, 425–436.
- Shideler, G. L., A. Slaczka, R. Unrug, and M. Wendorff (1975), Textural and mineralogical sorting relationship in Krosno Formation (Oligocene) turbidites, Polish Carpathian Mountains, *J. Sediment. Petrol.*, *45*, 44–56.
- Slingerland, R. (1984), Role of hydraulic sorting in the origin of fluvial placers, *J. Sediment. Petrol.*, *54*, 137–150.
- Stokes, G. G. (1851), On the effect of the internal friction of fluids on the motion of pendulums, *Cambridge Philosophical Transactions*, *9*, 8–106.